

# Unimpeded Permeation of Water Through Helium-Leak-Tight Graphene-Based Membranes

R. R. Nair,<sup>1,2</sup> H. A. Wu,<sup>1,3</sup> P. N. Jayaram,<sup>2</sup> I. V. Grigorieva,<sup>1</sup> A. K. Geim<sup>1,2,\*</sup>

Permeation through nanometer pores is important in the design of materials for filtration and separation techniques and because of unusual fundamental behavior arising at the molecular scale. We found that submicrometer-thick membranes made from graphene oxide can be completely impermeable to liquids, vapors, and gases, including helium, but these membranes allow unimpeded permeation of water (H<sub>2</sub>O permeates through the membranes at least 10<sup>10</sup> times faster than He). We attribute these seemingly incompatible observations to a low-friction flow of a monolayer of water through two-dimensional capillaries formed by closely spaced graphene sheets. Diffusion of other molecules is blocked by reversible narrowing of the capillaries in low humidity and/or by their clogging with water.

Despite being only one atom thick, graphene is believed to be impermeable to all gases and liquids (1, 2), which makes it tempting to exploit this material as a barrier film. Because of the ways graphene can currently be mass produced (3), films made from graphene oxide (GO) present a particularly interesting candidate. By using this graphene derivative, it is possible to make laminates, which are a collection of micron-sized GO crystallites forming an interlocked layered structure (4–6). This structure resembles that of nacre and exhibits great mechanical strength and flexibility, even for films of submicron thickness (3–6). In this Report, we investigate molecular permeation through such films.

Figure 1A shows an example of the studied GO membranes that were prepared as follows (7): We employed Hummer's method to obtain graphite oxide that was dispersed in water by sonication to make a stable suspension of GO crystallites (4–6). We then used this suspension to produce laminates by spray- or spin-coating (7). Scanning electron microscopy and x-ray analysis reveal that such GO films have a pronounced layered structure (Fig. 1B) and consist of crystals with typical sizes  $L$  of a few micrometers, which are separated by a typical distance  $d$  of  $\sim 10$  Å (4–6). For permeation experiments, Cu foils of several centimeters in diameter were uniformly covered with the GO laminates. Then, we chemically etched Cu to produce apertures of diameter  $D \approx 1$  cm fully covered by freestanding GO films (fig. S1). Finally, a metal container was sealed by using the Cu disks (fig. S2). We studied membranes with thicknesses  $h$  from 0.1 to 10  $\mu\text{m}$ .

<sup>1</sup>School of Physics and Astronomy, University of Manchester, Manchester M13 9PL, UK. <sup>2</sup>Centre for Mesoscience and Nanotechnology, University of Manchester, Manchester M13 9PL, UK. <sup>3</sup>Department of Modern Mechanics, Chinese Academy of Sciences Key Laboratory of Mechanical Behavior and Design of Materials, University of Science and Technology of China, Hefei, Anhui 230027, China.

\*To whom correspondence should be addressed. E-mail: geim@manchester.ac.uk

Even submicrometer-thick membranes were strong enough to withstand a differential pressure  $\Delta P$  up to 100 mbar.

As an initial test, we filled the containers with various gases under a small overpressure ( $<100$  mbar) and recorded its changes over a period of several days. We observed no noticeable reduction in  $\Delta P$  for any tested gas including He, H<sub>2</sub>, N<sub>2</sub>, and Ar. This allowed an estimate for the upper limit on their permeation rates  $Pr$  as  $\approx 10^{-11}$  g/cm<sup>2</sup>·s·bar, which is close to the value reported for micron-sized “balloons” made from continuous graphene monolayers (1). In

an alternative approach, we used mass spectrometry (fig. S2) and found no detectable permeation of He (Fig. 1D). The accuracy was limited only by digital noise of our He spectrometer and a slightly fluctuating background, which yielded  $Pr < 10^{-12}$  g/cm<sup>2</sup>·s·bar. Using hydrogen mass spectrometry, no permeation was found either, albeit the accuracy was three orders of magnitude lower than for He, due to a larger background. A 12- $\mu\text{m}$ -thick film of polyethylene terephthalate (PET) was used as a reference barrier and exhibited a He leakage rate 1000 times higher than our detection limit (Fig. 1D) yielding PET's bulk permeability  $\Pi_{\text{He}} = Pr \cdot h \approx 10^{-11}$  mm·g/cm<sup>2</sup>·s·bar, in agreement with literature values. The measurements set up an upper limit on  $\Pi_{\text{He}}$  for GO laminates as  $\approx 10^{-15}$  mm·g/cm<sup>2</sup>·s·bar; that is, our submicrometer-thick films provide a higher He gas barrier than 1-mm-thick glass (8).

To evaluate the permeation barrier for liquid substances, we employed weight-loss measurements. Figure 2 shows examples for evaporation rates from a metal container with an aperture covered by a 1- $\mu\text{m}$ -thick GO membrane. No weight loss could be detected with accuracy of  $<1$  mg for ethanol, hexane, acetone, decane, and propanol in the measurements lasting several days (7). This sets an upper limit for their  $\Pi$  as  $\approx 10^{-11}$  mm·g/cm<sup>2</sup>·s·bar. Unexpectedly, we observed a huge weight loss if the container was filled with water. Moreover, the evaporation rate was practically the same as in the absence of the GO film; that is, for the open aperture (Fig. 2A and fig. S3).

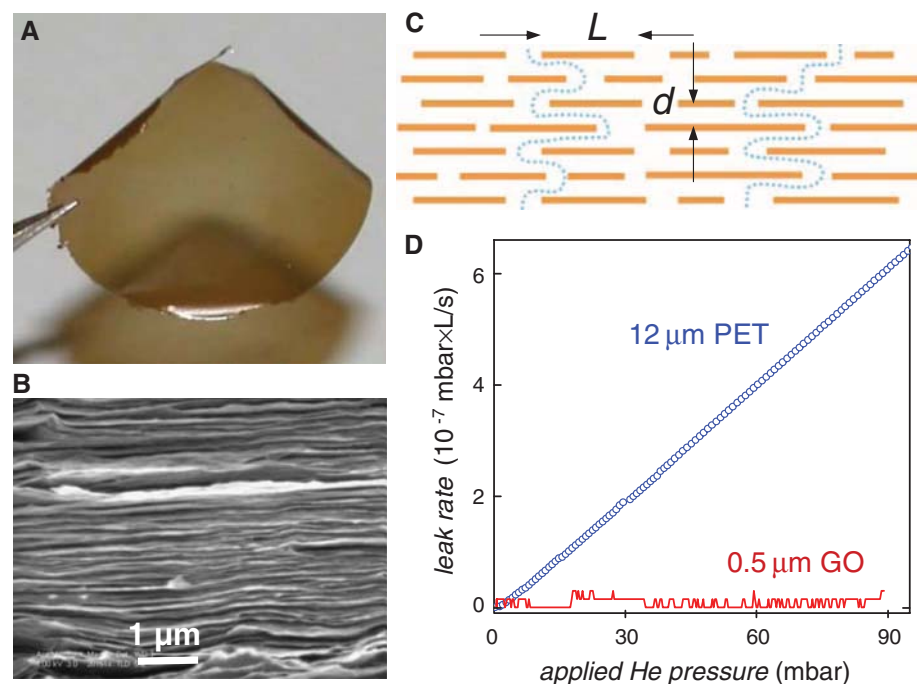


**Fig. 1.** He-leak-tight GO membranes. (A) Photo of a 1- $\mu\text{m}$ -thick GO film peeled off of a Cu foil. (B) Electron micrograph of the film's cross section. (C) Schematic view for possible permeation through the laminates. Typical  $L/d$  is  $\sim 1000$ . (D) Examples of He-leak measurements for a freestanding submicrometer-thick GO membrane and a reference PET film (normalized per square centimeter).

The latter was confirmed directly by using the same aperture with and without a GO cover. Furthermore, the same membrane could be used many times for different liquids, always exhibiting unimpeded and zero evaporation for H<sub>2</sub>O and other molecules, respectively. Also, after measurements with water, we checked the membranes for a He leak and found none. Only if we increased  $h$  to several micrometers could we observe a partial inhibition of water evaporation from the container (fig. S5), which yielded  $\Pi_{\text{H}_2\text{O}} \approx 10^{-5}$  mm·g/cm<sup>2</sup>·s·bar; that is, water permeates through GO films more than 10 orders of magnitude faster than He (Fig. 2B).

To elucidate the origin of the fast transport of water vapor through otherwise leak-tight GO films, we have carried out a number of additional experiments. First, we reduced GO by annealing it at 250°C in a hydrogen-argon atmosphere (5). The membranes became fragile and required extreme care to avoid cracks but nonetheless became 100 times less permeable to water (Fig. 2A). This can be attributed to structural changes such that  $d$  decreased from  $\approx 10$  to 4 Å, as shown by x-ray analysis and in agreement with earlier reports (9, 10). The importance of the interlayer distance was also witnessed when the partial pressure of water inside the container was reduced (fig. S3). If the pressure dropped below 10 mbar, the permeation stopped (7), which again can be explained by changes in  $d$  in low humidity. X-ray analysis of GO in various humidity shows that this blockage occurs when  $d$  falls below  $\approx 7$  Å (11, 12). The process of opening and closing the GO capillaries was found reversible with varying humidity (7).

Further insights into the permeation mechanism come from experiments using mixtures of H<sub>2</sub>O with other gases and liquids. Mass spectroscopy showed that, in the presence of saturated water vapor, He did permeate through

GO membranes (fig. S4). However, its rate was  $\approx$ five orders of magnitude slower than that of H<sub>2</sub>O, in agreement with the rate calculated for He diffusion through an equivalent column of water (7). For other molecules (for example, ethanol and H<sub>2</sub>), we were unable to detect their permeation along with H<sub>2</sub>O (7). This shows that, despite somewhat larger  $d$  in high humidity, the intercalating water blocks, or at least impedes, other molecules from moving through GO.

In another series of experiments, we investigated why water permeated through GO film as fast as through an open aperture. To this end, membranes were placed on a support grid that allowed us to apply a water pressure of several bars without damaging them. The large  $\Delta P$  did not result in any noticeable increase in  $Pr$  with respect to water vapor. On the other hand, if we increased humidity outside the container,  $Pr$  decreased. Furthermore, if we blew air at the GO membrane, this increased the weight loss rate. Also,  $Pr$  increased if the container was heated (we could increase temperature up to 40°C, above which the membranes had a tendency to develop cracks). The same changes in  $Pr$  happened when we changed temperature of the membrane only, without heating water inside. In all the cases,  $Pr$  changed similarly to the evaporation rate from an open-water surface under similar conditions. This suggests that permeation of water through our membranes was limited by evaporation from the wetted surface of GO.

To explain our findings, we recall that GO laminates consist of crystallites stacked on top of each other (Fig. 1C). The groups (for instance, hydroxyl, epoxy, etc.) attached to graphene sheets are responsible (9–12) for keeping the relatively large spacing  $d$  (fig. S6). Importantly, such groups tend to cluster and leave large, percolating regions of graphene sheets not oxidized (5, 7, 13, 14). Therefore, GO laminates are likely to have empty

spaces formed between nonoxidized regions of graphene sheets (fig. S6). Because  $d$  for reduced GO is  $\approx 4$  Å, the empty space's width  $\delta$  can be estimated as  $\approx 5$  Å, which is sufficient to accommodate a monolayer of water (15, 16). We speculate that these empty spaces form a network of pristine-graphene capillaries within GO laminates. By invoking the same water-permeation mechanism as previously used for small-diameter carbon nanotubes and hydrophobic nanopores (17–25), we suggest that the two-dimensional (2D) graphene nanocapillaries allow low-friction flow of monolayer water. At the same time, the oxidized regions that strongly interact with intercalating water are unlikely (7) to contribute to water permeation and, in our model, serve as spacers for the 2D capillary network (fig. S6).

To support our explanation, we used molecular dynamics (MD) simulations (7). Because a graphene monolayer is essentially impermeable, molecular transport in GO laminates should involve a permeation path through the network of graphene nanocapillaries as discussed above (Fig. 1C and fig. S6). The bottleneck in this process is the passage between graphene sheets separated by  $d \ll L$  (figs. S6 and S7). For  $d \leq 6$  Å (including the van der Waals thickness of graphene), our MD simulations show that water cannot fill the capillaries. On the other hand, for  $d \geq 10$  Å, two layers of water start forming between the sheets. For intermediate  $d$ , water rushes into the capillaries (21, 22) and forms a highly ordered monolayer shown (Fig. 2B, inset), in agreement with the previous analysis for 2D capillaries (15, 16). Furthermore, the simulations enabled us to estimate the involved capillary pressure as on the order of 1000 bars (7), in qualitative agreement with the estimates based on van der Waals interaction between water and graphite (26). Such capillary pressures explain why the water permeation in our experiments was insensitive to  $\Delta P$  of several bars. Similar to the case of nanotubes, our simulated water can move anomalously fast, with velocities reaching meters per second and, thus, sufficient to sustain the observed permeation rates (fig. S8). Finally, we mimicked the oxidized graphene regions by adding arrays of epoxy groups to the simulated capillaries and found the water permeation being strongly impeded for all  $d \leq 10$  Å.

The observed unimpeded evaporation of water through He-leak-tight membranes resembles the permeation of protons (atomic hydrogen) through thin films of transition metals, a phenomenon known as superpermeability (27). Despite the analogy, our phenomenon is different and explained by a network of graphene nanocapillaries formed within GO laminates, which are filled with monolayer water under ambient conditions. A capillary-like pressure provides a sufficient flow to keep the external GO surface wetted so that the observed permeability is effectively limited by the surface evaporation (28). The described GO membranes can be used as barrier films in the design of filtration and separation materials and for selective removal of water (7).

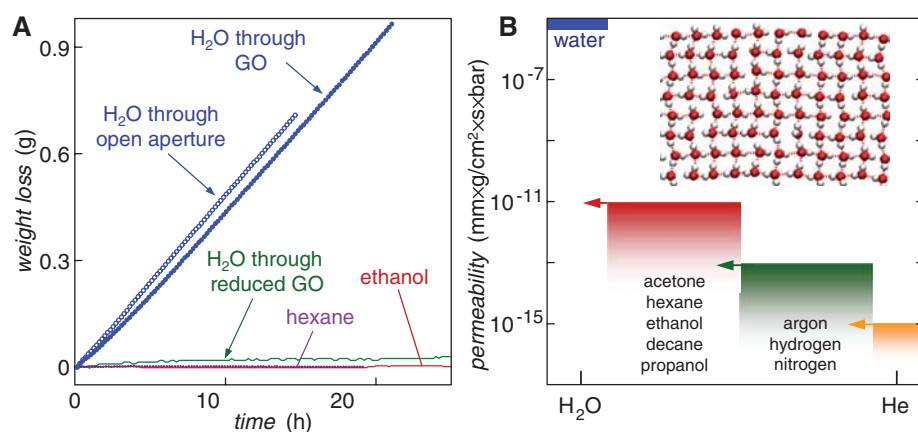


**Fig. 2.** Permeation through GO. **(A)** Weight loss for a container sealed with a GO film ( $h \approx 1$   $\mu\text{m}$ ; aperture's area  $\approx 1$   $\text{cm}^2$ ). No loss was detected for ethanol, hexane, etc. (7), but water evaporated from the container as freely as through an open aperture (blue curves). The measurements were carried out at room temperature in zero humidity. **(B)** Permeability of GO paper with respect to water and various small molecules (arrows indicate the upper limits set by our experiments). (Inset) Schematic representation of the structure of monolayer water inside a graphene capillary with  $d = 7$  Å, as found in our MD simulations (7).

## References and Notes

1. J. S. Bunch *et al.*, *Nano Lett.* **8**, 2458 (2008).
2. O. Leenaerts, B. Partoens, F. M. Peeters, *Appl. Phys. Lett.* **93**, 193107 (2008).
3. A. K. Geim, *Science* **324**, 1530 (2009).
4. D. A. Dikin *et al.*, *Nature* **448**, 457 (2007).
5. G. Eda, M. Chhowalla, *Adv. Mater.* **22**, 2392 (2010).
6. J. T. Robinson *et al.*, *Nano Lett.* **8**, 3441 (2008).
7. See supporting material on Science Online.
8. F. J. Norton, *J. Am. Ceram. Soc.* **36**, 90 (1953).
9. M. J. McAllister *et al.*, *Chem. Mater.* **19**, 4396 (2007).
10. H. K. Jeong *et al.*, *Chem. Phys. Lett.* **470**, 255 (2009).
11. A. Lerf *et al.*, *J. Phys. Chem. Solids* **67**, 1106 (2006).
12. S. Cerveny, F. Barros-Bujans, Á. Alegría, J. Colmenero, *J. Phys. Chem. C* **114**, 2604 (2010).
13. N. R. Wilson *et al.*, *ACS Nano* **3**, 2547 (2009).
14. D. Pacilé *et al.*, *Carbon* **49**, 966 (2011).
15. R. Zangi, A. E. Mark, *Phys. Rev. Lett.* **91**, 025502 (2003).
16. N. Giovambattista, P. J. Rosky, P. G. Debenedetti, *Phys. Rev. Lett.* **102**, 050603 (2009).
17. J. K. Holt *et al.*, *Science* **312**, 1034 (2006).
18. M. Majumder, N. Chopra, R. Andrews, B. J. Hinds, *Nature* **438**, 44 (2005).
19. X. Peng, J. Jin, Y. Nakamura, T. Ohno, I. Ichinose, *Nat. Nanotechnol.* **4**, 353 (2009).
20. X. Qin, Q. Yuan, Y. Zhao, S. Xie, Z. Liu, *Nano Lett.* **11**, 2173 (2011).
21. M. Whitby, N. Quirke, *Nat. Nanotechnol.* **2**, 87 (2007).
22. J. C. Rasaiah, S. Garde, G. Hummer, *Annu. Rev. Phys. Chem.* **59**, 713 (2008).
23. J. Köfinger, G. Hummer, C. Dellago, *Proc. Natl. Acad. Sci. U.S.A.* **105**, 13218 (2008).
24. J. A. Thomas, A. J. H. McGaughey, *Phys. Rev. Lett.* **102**, 184502 (2009).
25. Y. Li, J. Xu, D. Li, *Microfluid. Nanofluid.* **9**, 1011 (2010).
26. F. Caupin, M. W. Cole, S. Balibar, J. Treiner, *Europhys. Lett.* **82**, 56004 (2008).
27. A. I. Livshits, M. E. Notkin, V. I. Pistunovich, M. Bacal, A. O. Busnyuk, *J. Nucl. Mater.* **220-222**, 259 (1995).
28. N. Goedecke, J. Eijkel, A. Manz, *Lab Chip* **2**, 219 (2002).

**Acknowledgments:** This work was supported by the Engineering and Physical Research Council (UK), the U.S. Office of Naval Research, the U.S. Air Force Office of Scientific Research, the Royal Society, and the Körber Foundation. We thank K. S. Novoselov, E. Hill, P. Blake, S. Neubeck, and R. Joshi for their help. H.A.W. is grateful for support from the National Science Foundation of China and Oversea Academic Training Funds—University of Science and Technology of China.

**Supporting Online Material**

[www.sciencemag.org/cgi/content/full/335/6067/442/DC1](http://www.sciencemag.org/cgi/content/full/335/6067/442/DC1)

Materials and Methods

SOM Text

Figs. S1 to S8

References (29–38)

25 July 2011; accepted 17 November 2011

10.1126/science.1211694



www.sciencemag.org/cgi/content/full/335/6067/442/DC1

## Supporting Online Material for

### **Unimpeded Permeation of Water Through Helium-Leak-Tight Graphene-Based Membranes**

R. R. Nair, H. A. Wu, P. N. Jayaram, I. V. Grigorieva, A. K. Geim\*

\*To whom correspondence should be addressed. E-mail: [geim@manchester.ac.uk](mailto:geim@manchester.ac.uk)

Published 27 January 2012, *Science* **335**, 442 (2012)  
DOI: 10.1126/science.1211694

**This PDF file includes:**

Materials and Methods  
SOM Text  
Figs. S1 to S8  
Full Reference List

## Materials and Methods

### Fabrication of GO membranes

Graphite oxide was prepared from natural graphite flakes by treating them with potassium permanganate and sodium nitrate in concentrated sulphuric acid (29). Individual graphene oxide (GO) sheets were exfoliated by dissolving graphite oxide in water with the help of ultrasound, and bulk residues were then removed by centrifugation. To fabricate GO membranes, we used the above suspension to spin- or spray-coat a 25- $\mu\text{m}$ -thick copper foil. To increase the deposition rate, the disks were usually heated to  $\approx 50^\circ\text{C}$ . Freestanding GO membranes of  $\sim 1\text{cm}$  in diameter were prepared by etching away a central part of the copper foil in nitric acid. Finally, the membranes were cleaned in distilled water and dried on a hot plate ( $< 50^\circ\text{C}$ ). Steps involved in the fabrication process are schematically shown in fig. S1.

Furthermore, we could produce freestanding membranes by vacuum filtration of the GO suspension through Anodisc filters ( $0.2\ \mu\text{m}$  pore size). The latter membranes were used in the experiments to apply a high water pressure and for X-ray analysis.

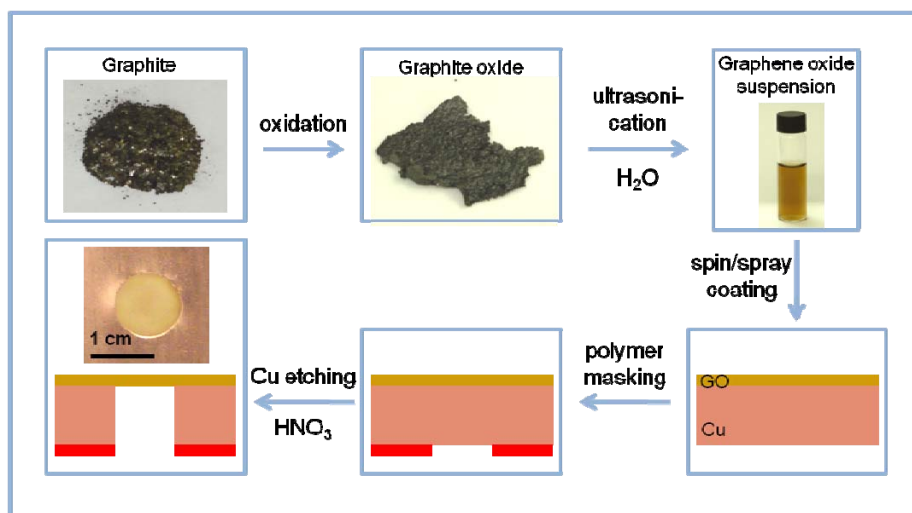


Fig. S1. Fabrication procedures for GO membranes.

### Experimental setup

Metal containers for permeation experiments were fabricated from an aluminum alloy and sealed by using two O rings that clamped the Cu foil from both sides, as shown schematically in fig. S2. The studied GO membranes could withstand a differential pressure of up to 0.1 bar, which indicates strong adhesion between GO and the copper surface.

For gravimetric measurements (see Fig. S2A), the containers were specially designed to minimize their mass. The weight loss was monitored by using a computer-controlled precision balance (ADAM Equipment Ltd; accuracy 1 mg). All the gravimetric experiments were carried out in an argon atmosphere in a glove box with a negligible water pressure ( $< 10^{-3}$  mbar). If the containers were sealed with submicron GO membranes, no weight loss could be detected for any liquid other than water. For the case of an open aperture, evaporation rates for other liquids were higher than for water (for example,  $\approx 1.3$ , 6.0 and 8.3 mg/h/mm<sup>2</sup> for ethanol, hexane and acetone

at room temperature ( $T$ ), respectively). To calculate the upper limits for permeability of the liquids (shown in Fig. 2b), we used their partial pressures at room  $T$ .

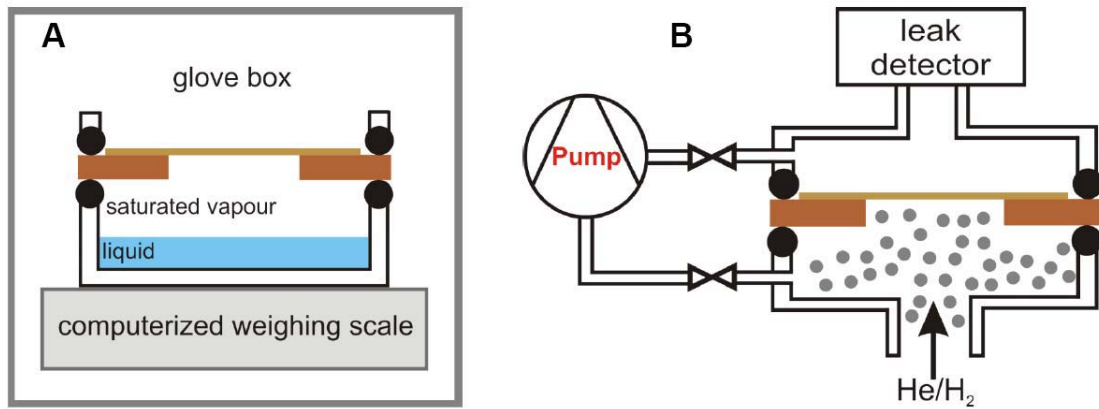


Fig. S2. Schematics of our experimental setups. (A) Permeation measurements by the gravimetric method. (B) Permeation of helium and hydrogen was studied by mass spectrometry.

In additional experiments, we made sure that water did not ‘wick’ between GO and Cu. To this end, we evaporated a thick aluminum film outside the freestanding part of the GO membrane to seal its boundary so that no water could possibly evaporate from the edges of GO membranes. This was further crosschecked by using a specially-designed container that did not allow any weight loss, even if water could evaporate from the membrane’s periphery. Furthermore, the evaporation rate did not change if we turned the container upside down (that is, the liquid rather than vapor was in direct contact with the GO membrane). This observation is consistent with the high capillary pressure (see below), and our model in which the water loss rate is limited by evaporation from the wetted top surface of GO membranes.

For mass spectrometry and pressure monitoring, we made larger containers that incorporated inlets with the standard vacuum flanges to allow pumping, pressure gauges and controllable supply of gases (fig. S2B). As a mass spectrometer, we used helium-leak detector INFICON UL200 which allowed detection of helium and hydrogen.

## SOM Text

### #1 Influence of humidity on water permeation through GO membranes

We have studied the evaporation rate as a function of water’s partial pressure  $\Delta P$ . At room  $T$ , 100% relative humidity (RH) corresponds to  $\approx 23$  mbar of H<sub>2</sub>O. We could change RH (and, hence,  $\Delta P$  for water) inside our sealed container by using various saturated salt solutions (11,30). To this end, the calibrated salts were wetted with distilled water and placed at the bottom of the container without any contact with the studied membranes. For each salt as well as for distilled water, we measured the water permeation by the weight loss method. The salts we used were potassium chloride that provides 85% RH, sodium chloride (75%), magnesium nitrate (55%), potassium carbonate (43%), magnesium chloride (33%), potassium acetate (23%) and lithium chloride (11%). Figure S3 shows the influence of RH (that is, differential vapor pressure  $\Delta P$ ) on water permeation through one of our GO membrane (thickness  $h \approx 0.5\mu\text{m}$ ). For comparison, we

also plot the measured evaporation rate for the same aperture but in the absence of the GO film (it was mechanically removed).

For 100% RH, both open aperture and GO membrane exhibit nearly the same permeation rate as shown in figure S3 and, also, Fig. 2a of the main text. However, for lower humidity the permeation rate through GO starts showing strong deviations from that through the open aperture. In the latter case, the evaporation rate decreases linearly with decreasing RH, as expected. In contrast, the GO membrane exhibits a strongly nonlinear behavior and, for RH below 50%, the water permeation rate through the membrane becomes much smaller than through the same open aperture. The permeation stops at RH below 20% (fig. S3). The RH required for the stoppage varied from sample to sample and, for some membranes, it stopped at RH as high as 30%. The blocked (dried-out) membranes fully recovered to their initial highly-permeable state after a prolonged (>1day) exposure to 100% humidity.

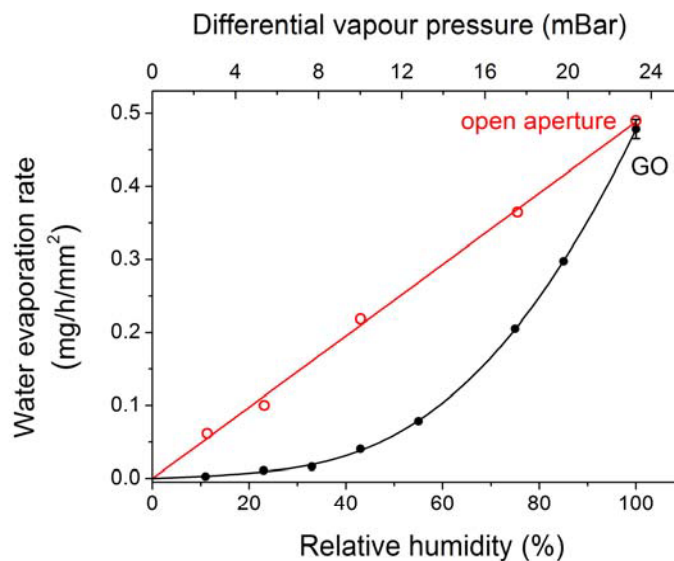


Fig. S3. Water permeation through an open aperture and the same aperture covered with a 0.5- $\mu\text{m}$ -thick GO membrane. Solid lines are guides to the eye. At 100% RH, the permeations rates with and without a thin GO membrane nearly coincide. The rates become notably different for thicker membranes (see further).

The blockage induced by low RH can be attributed to changes in GO's interlayer spacing  $d$  as it happened when GO membranes were reduced by annealing (main text). Indeed, it was previously reported (11,12) that graphite oxide exhibited a decrease in  $d$  with decreasing RH such that  $d$  changed from  $\approx 11$  to  $7\text{\AA}$  for RH varying from 100 to 30%, respectively. To confirm this effect for our GO films, we have carried out their X-ray analysis at various humidity and found  $d$  close to the values reported in (11). Therefore, it is clear that RH controls the interlayer separation in our GO laminates too. For 100% humidity, the observed separation of  $\approx 10\text{\AA}$  should be sufficient to accommodate one monolayer of  $\text{H}_2\text{O}$  molecules and allow their diffusion. For lower RH, this freedom of movement becomes restricted because of smaller  $d$ . As more and more capillaries dry out and become effectively closed, the water permeation can be expected to stop. This is our model discussed in the main text, supported by molecular dynamics (MD) simulations and explained in more detail below.

## #2 Length of 2D capillaries and flow velocity

Figure 1c of the main text shows schematically the suggested permeation path for water through GO membranes. They have a layered structure made of graphene sheets separated by an interlayer distance  $d$  between  $\approx 7$  and  $11\text{\AA}$ , depending on the humidity (see #1). Taking into account that the electronic clouds around graphene sheets extend over a distance of  $a \approx 3.5\text{\AA}$ , the above separation  $d$  translates into an ‘empty’ space of width  $\delta = (d - a) = 3$  to  $7\text{\AA}$ , which can be available for other molecules to diffuse.

With reference to Fig. 1c, the complete path of water through a GO film of thickness  $h$  involves a number of turns  $N = h/d$ , and each turn involves a capillary length  $L \sim 1\mu\text{m}$  (we assume that the crystallites have the same typical width and length). Therefore, the total length  $l$  of each effective channel is given by  $N \times L$ , yielding  $l \sim 1$  mm for our typical  $1\text{-}\mu\text{m}$ -thick membrane. The total number of the channels per unit area can be estimated as by  $1/L^2$ , that is, our membranes with a typical area of  $\approx 1\text{cm}^2$  effectively contain  $\sim 10^8$  parallel 2D channels. Nanocapillaries occupy a relatively small part of the total membrane area ( $\pi D^2/4$ ) and this fraction  $v$  can be estimated as  $\delta/L \sim 0.1\%$ . To sustain the observed evaporation rate  $Q \approx 50\text{mg/h}$  per  $\text{cm}^2$  at room  $T$  (main text and below), it requires a flow inside the capillaries with velocity  $V = Q/v\rho$  where  $\rho$  is the water density. This yields  $V$  of the order of  $0.01$  cm/s. Note that this is a lower bound for  $V$  because some inner capillary area is blocked by epoxy, hydroxyl and other functional groups.

## #3 Permeation of helium in high humidity

As the distance  $d$  between graphene sheets strongly depends on humidity, the suggested permeation mechanism implies that other molecules may start permeating through GO membranes under high humidity conditions when the graphene capillaries become wider. Although they are filled with intercalating water, other atoms and molecules may diffuse through water. To check this hypothesis, we have carried out additional experiments in which He (20 mbar) was added to the saturated water vapor. Figure S4 shows the observed He-leak rate as a function of time for a  $1\text{-}\mu\text{m}$ -thick GO membrane. One can see that, in high humidity, helium indeed starts permeating through GO. Initially its speed increases with time as the membrane gets hydrated and, after a few hours, the leak saturates to practically a constant value. For comparison, the figure also shows that the same GO membrane was leak tight with respect to dry helium.

The observed leak for the case of humid He can be explained by diffusion of He atoms through an equivalent column of water. As shown in #2, our capillaries effectively add up to a water column of approximately 1 mm high with a cross-section of  $\approx 10^{-3}\text{ cm}^2$ . The diffusion coefficient of He in water is known to be  $\approx 6 \times 10^{-5}\text{ cm}^2/\text{s}$  (31). It is straightforward to estimate that the He leak rate through the water column is of the same order of magnitude as the rate observed in fig. S4.

The observed permeation rates for He through intercalating water are low, even in the case of high humidity and, therefore, one can generally expect that under the same circumstances larger molecules will diffuse even slower than helium. He mass spectroscopy is known to provide an exceptionally high sensitivity and, not surprisingly, our other techniques (including  $\text{H}_2$  mass spectroscopy) did not allow detection of larger molecules escaping through GO membranes exposed to high humidity. Another example we studied was a mixture of water and ethanol. Starting with a 50-50 solution, we observed that water vapor escaped from the container sealed with a GO membrane (approximately 2 times slower than in the case of pure water). The detected weight loss changed in time, according to a partial pressure of water inside the container, until the concentration of ethanol reached  $\approx 80\%$  and the capillaries become sealed because of low

humidity. These experiments using He, H<sub>2</sub> and ethanol confirm that, in high humidity when  $d$  is large, the intercalating water at least impedes larger molecules from moving through graphene nanocapillaries.

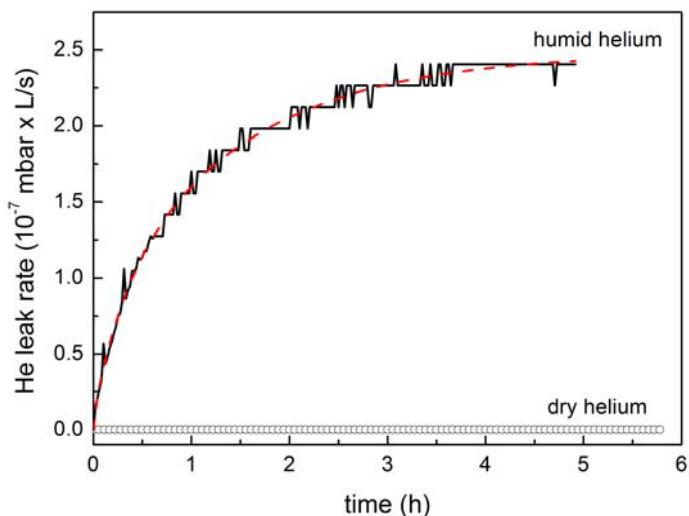


Fig. S4. He leak rate as a function of time for a  $\mu\text{m}$ -thick GO membrane in zero and high humidity ( $1\text{ cm}^2$  area). The dashed red curve is a guide to the eye.

#### #4 Effect of membrane thickness on water permeation

The observation of the same evaporation rates from an open container and the same container covered with a  $0.5\text{-}\mu\text{m}$ -thick GO membrane (Figs. 2a, S3) poses an important question: at what thickness does the presence of the GO films start playing any role? To answer this question, we employed GO membranes with  $h$  up to  $10\text{ }\mu\text{m}$ , the maximum thickness that we could achieve by spray/spin-coating.

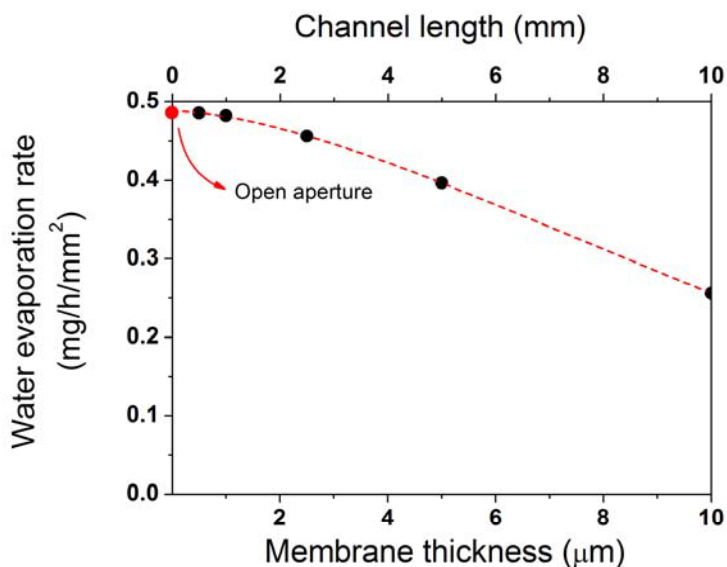


Fig. S5. Dependence of the evaporation rate on GO membrane's thickness (symbols). The dashed curve is a guide to the eye. The upper axis shows the effective channel length  $l$  that is calculated as described in #2.

Figure S5 shows water loss rate  $Q$  as a function of  $h$ . The measurements were carried out by the same gravimetric method under the identical conditions. It is clear that the vapor barrier is practically absent for the submicron GO membranes but gradually builds up for thicker films. For our thickest membrane, the flow is impeded by a factor of two. The observed changes in the evaporation rate have allowed us to estimate the permeation value for bulk GO, which is given in the main text.

#### #5 Comparison with classical flow equations

It is instructive to compare the experimentally observed permeation rate with that expected from the classical equations for the given sizes of nanocapillaries. If we assume that H<sub>2</sub>O permeates through our GO membranes as a gas and, therefore, the Knudsen regime is applicable (diffusion is limited by collisions with graphene walls), the mass flow per unit area can be estimated as

$$Q \approx \delta^3 \left( \frac{1}{L^2} \right) \left( \frac{M}{RT} \right)^{1/2} \left( \frac{\Delta P}{l} \right)$$

where  $M$  is the molecular weight of water,  $R$  the gas constant and  $1/L^2$  the area density of 2D channels. For simplicity, let us consider our thickest membrane ( $h \approx 10 \mu\text{m}$  and the effective channel length  $l \sim 10 \text{ nm}$ ), in which the observed weight loss becomes limited by GO properties rather than the aperture's area (fig. S5). At this thickness, the membranes allow flux  $Q \sim 25 \text{ mg/h per cm}^2$  (see fig. S5). On the other hand, the Knudsen formula for such membranes yields  $Q \sim 10^{-9} \text{ mg/h per cm}^2$ . This is ten orders of magnitude smaller than the H<sub>2</sub>O flux observed experimentally.

Alternatively, assuming that water inside our nanocapillaries behaves as a classical liquid, we can employ the Hagen-Poiseuille equation

$$Q \approx \delta^3 \left( \frac{1}{12\eta} \right) \left( \frac{1}{L} \right) \left( \frac{\Delta P}{l} \right) \rho$$

where  $\eta$  is the viscosity of bulk water (1 mPa·s) and  $\rho$  its density. For the other parameters remaining the same, the latter equation yields  $Q \sim 10^{-6} \text{ mg/h per cm}^2$ , that is, nanoconfined water exhibits a flow enhanced by a factor  $\Theta \sim 10^7$  with respect to the classical laminar regime. In both equations above, we have assumed the differential pressure  $\Delta P$  to be 23 mbar (100% RH). However, monolayer water interacts with the graphene surface and, according to van-der-Waals-energy considerations (26), this interaction should lead to a high capillary-like pressure  $P$  of  $\approx 10^3\text{--}10^4 \text{ bar}$ . This is in conceptual agreement with our molecular dynamics (MD) simulations below, which yield  $P$  of the order of  $10^3 \text{ bar}$ . Therefore, it is appropriate to use the latter value as the driving pressure  $\Delta P$  in the Hagen-Poiseuille equation. Then, our experiments infer an enhancement factor  $\Theta$  of only a few hundred, in agreement with the enhancement factor that was recently (20,32) revised for the case of sub-1-nm nanotubes with one file of moving water. Furthermore, the enhanced water flow in nanoporous materials is often described by the slip length  $l_s$ , a parameter describing the lowered friction between water and capillary walls. Our experiments allow an estimate for  $l_s \sim \Theta \cdot \delta/8 \approx 10\text{--}100 \text{ nm}$ , again in agreement with the most recent measurements for the correlated water flow in the 1D geometry (20).

Let us note that when using the Hagen-Poiseuille equation we assumed in there the viscosity of bulk water. The reason for this is that it is a convention in the carbon nanotube literature to calculate  $\Theta$  with respect to  $\eta$  for bulk water (17,18). This assumption is justified by the fact that the effective viscosity of nanoconfined water remains within a factor of 3 of its bulk

value (33). Moreover, it has recently been found that, for monolayer water,  $\eta$  returns to close to the bulk value (34).

#### #6 Atomistic simulations of water dynamics in 2D graphene capillaries

To gain a theory insight about water permeation through sub-1-nm-wide 2D capillaries, we employed classical MD simulations, which have previously been proven an efficient tool to investigate molecular transport at nanoscale. According to our model described in the main text, we simulated our nanocapillaries as being formed by two pristine-graphene sheets. ‘Oxidized’ regions play a role of spacers that keep graphene planes  $\approx 7$  to  $10\text{\AA}$  apart. Figure S6 illustrates this model further by showing the GO structure, according to its current understanding (4-6,13,14,35). There are pristine and oxidized regions on graphene sheets, which have a typical size of several nm (13,14,35). According to our MD analysis below,  $\text{H}_2\text{O}$  molecules can form a 2D network (15,16) between pristine-graphene sheets for  $d > 6\text{\AA}$  (central part in fig. S6). This monolayer water is expected to be highly mobile, similar to the case of the water files formed in small-diameter carbon nanotubes (17,18,20,21). Due to hydrogen bonding and a narrower space available for diffusion, water is expected to be less mobile within the oxidized regions that are randomly covered with epoxy, hydroxyl, etc. groups (fig. S6). This is also in agreement with our MD simulations using  $10\text{\AA}$  graphene capillaries covered with epoxy groups. If humidity becomes low so that GO films dry out, the nanocapillaries narrow in both oxidized and pristine regions. This narrowing of pristine-graphene nanocapillaries results in blocking of the water transport as schematically indicated by the dashed lines in fig. S6.

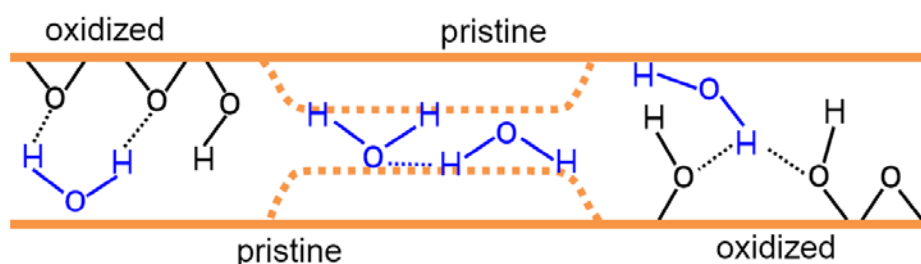


Fig. S6. Our model for graphene capillaries within GO films. When the pristine-graphene capillaries are wide open, monolayer water (two  $\text{H}_2\text{O}$  molecules are shown) can move through. In low humidity, the capillaries become narrower (dashed lines), and there is not enough van der Waals distance to graphene walls to accommodate a water molecule.

Our simulations of water dynamics through graphene nanocapillaries were carried out by using the LAMMPS software package from Sandia National Laboratories (36). Figure S7 shows the setup that consists of two graphene reservoirs and a connecting 2D graphene capillary. All the carbon atoms in the model are assumed static. For water simulations, we have employed the SPC/E model (37) with the O-H bond length of  $1.0\text{\AA}$  and the H-O-H angle of  $109.47^\circ$ . The harmonic style was used for both bond and angle potentials (see LAMMPS Manual). The charges on the oxygen site and the hydrogen sites were chosen  $-0.8476 e$  and  $+0.4238 e$ , respectively ( $e$  is the free electron charge). The electrostatic interaction was modeled by using the Coulomb potential. Van der Waals interactions between atoms were described by a 12-6 Lennard-Jones (LJ) potential with parameters  $\epsilon_{\text{O-O}} = 0.1553 \text{ kcal/mol}$  and  $\sigma_{\text{O-O}} = 3.166\text{\AA}$ . The particle-particle mesh solver was applied to account for the truncation of the long-range electrostatic

forces (36). The LJ potential parameters for the C-O interaction were calculated by the Lorentz-Berthelot combining rules, and we used the same parameters as in ref. 38, that is,  $\epsilon_{C-C} = 0.0553 \text{ kcal/mol}$ ,  $\sigma_{C-C} = 3.4 \text{ \AA}$ ,  $\epsilon_{C-O} = 0.0927 \text{ kcal/mol}$  and  $\sigma_{C-O} = 3.283 \text{ \AA}$ . The cut-off distance for all LJ potentials was chosen  $10 \text{ \AA}$ . For computational efficiency, LJ parameters for the atomistic interactions involving hydrogen atoms were set to zero. The simulations were carried out for  $T = 300 \text{ K}$ .

To account for the dimensionality, we used the periodic boundary conditions with a period of  $\approx 21 \text{ \AA}$  (out-of-plane direction in fig. S7). The length of the 2D capillary in figure S7 is  $\approx 74 \text{ \AA}$  (30 graphene hexagons). The length of the left reservoir is  $\approx 50 \text{ \AA}$  and its height  $\approx 75 \text{ \AA}$ . The MD simulations were carried out for 4 different widths  $d$  of the 2D slit: namely, 6, 6.5, 7 and  $7.5 \text{ \AA}$  (measured between the centers of carbon atoms). A fixed number of water molecules were initially put in the left reservoir, while the capillary and the right reservoir were kept empty. If a water molecule passed through the channel, it disappeared ('evaporated') at the other end, in the right reservoir. The number of water molecules entering the right reservoir is shown as a function of time in figure S8. Our MD simulations revealed that water molecules tended to enter the capillary and initially moved through it with a velocity of  $\approx 20 \text{ m/s}$  (fig. S8). They reached the evaporation point after  $\sim 0.4 \text{ ns}$  for all the channels with  $d > 6 \text{ \AA}$ . On the other hand, the  $6 \text{ \AA}$  channel did not allow any noticeable permeation. This indicates that  $d > 6 \text{ \AA}$  is necessary to accommodate a single layer of water between the simulated graphene sheets.

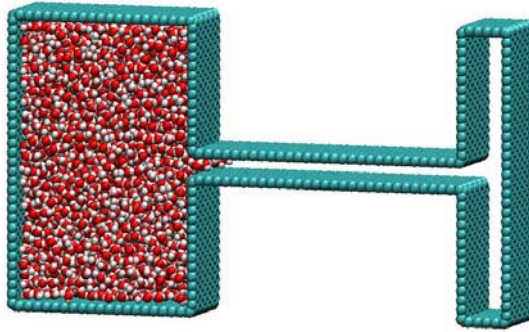


Fig. S7. Model used to simulate water-molecule dynamics in 2D graphene nanocapillaries.

The initial density of water in the reservoir was chosen larger than that of bulk water. Still, the differential pressure could not cause any flow through the  $6 \text{ \AA}$  slit. For the wider capillaries, the density of water molecules in the left reservoir gradually decreased because of the evaporation process and, therefore, the differential pressure decreased too. This is why water molecules moved fast during the first 2 ns and then slowed down (fig. S8). Importantly, after 5ns, the water density in the left reservoir became close to or smaller than that of bulk water. In this regime, the initial hydrostatic pressure is no longer the driving force but water molecules still fill in and move through the capillary.

The fact that the water fills the 2D channel even under a negative pressure in the left reservoir indicates an additional driving mechanism that can be attributed to the interaction between monolayer water and graphene walls in the capillary, as discussed above. We have carried out further MDS to estimate this effective capillary pressure  $P$ . To this end, simulations were restarted from molecular configurations reached after 10ns, when the channel was fully filled, and an additional force was applied to all oxygen atoms in the direction against the flow.

This mimics a gravitational force and can directly be translated into an extra capillary pressure  $P$  in the slit. We found that if  $P$  exceeded  $\approx 500$  bars, water molecules in the channel were pulled back to the left reservoir, and the 2D capillary started to dry out. The found value of  $P$  in our 1-nm-sized slit is in qualitative agreement with the estimate (26) by using the van-der-Waals interaction energy between water and graphite.

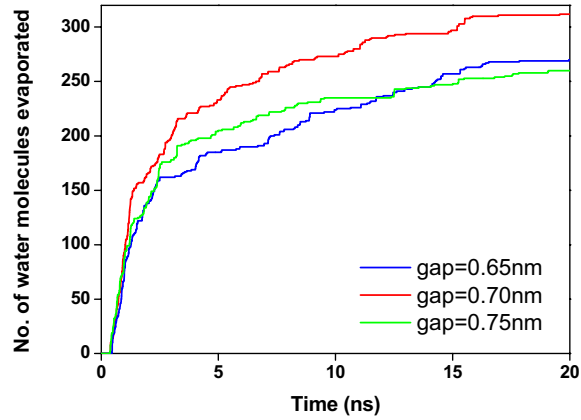


Fig. S8. The number of water molecules reaching the right reservoir as a function of time. Different colors correspond to different channel widths  $d$ .

## References and Notes

1. J. S. Bunch *et al.*, Impermeable atomic membranes from graphene sheets. *Nano Lett.* **8**, 2458 (2008). [doi:10.1021/nl801457b](https://doi.org/10.1021/nl801457b) [Medline](#)
2. O. Leenaerts, B. Partoens, F. M. Peeters, Graphene: A perfect nanoballoon. *Appl. Phys. Lett.* **93**, 193107 (2008). [doi:10.1063/1.3021413](https://doi.org/10.1063/1.3021413)
3. A. K. Geim, Graphene: Status and prospects. *Science* **324**, 1530 (2009). [doi:10.1126/science.1158877](https://doi.org/10.1126/science.1158877) [Medline](#)
4. D. A. Dikin *et al.*, Preparation and characterization of graphene oxide paper. *Nature* **448**, 457 (2007). [doi:10.1038/nature06016](https://doi.org/10.1038/nature06016) [Medline](#)
5. G. Eda, M. Chhowalla, Chemically derived graphene oxide: Towards large-area thin-film electronics and optoelectronics. *Adv. Mater.* **22**, 2392 (2010). [doi:10.1002/adma.200903689](https://doi.org/10.1002/adma.200903689) [Medline](#)
6. J. T. Robinson *et al.*, Wafer-scale reduced graphene oxide films for nanomechanical devices. *Nano Lett.* **8**, 3441 (2008). [doi:10.1021/nl8023092](https://doi.org/10.1021/nl8023092) [Medline](#)
7. See supporting material on *Science Online*.
8. F. J. Norton, Helium diffusion through glass. *J. Am. Ceram. Soc.* **36**, 90 (1953). [doi:10.1111/j.1151-2916.1953.tb12843.x](https://doi.org/10.1111/j.1151-2916.1953.tb12843.x)
9. M. J. McAllister *et al.*, Single sheet functionalized graphene by oxidation and thermal expansion of graphite. *Chem. Mater.* **19**, 4396 (2007). [doi:10.1021/cm0630800](https://doi.org/10.1021/cm0630800)
10. H. K. Jeong *et al.*, Thermal stability of graphite oxide. *Chem. Phys. Lett.* **470**, 255 (2009). [doi:10.1016/j.cplett.2009.01.050](https://doi.org/10.1016/j.cplett.2009.01.050)
11. A. Lerf *et al.*, Hydration behavior and dynamics of water molecules in graphite oxide. *J. Phys. Chem. Solids* **67**, 1106 (2006). [doi:10.1016/j.jpcs.2006.01.031](https://doi.org/10.1016/j.jpcs.2006.01.031)
12. S. Cervený, F. Barros-Bujans, Á. Alegría, J. Colmenero, Dynamics of water intercalated in graphite oxide. *J. Phys. Chem. C* **114**, 2604 (2010). [doi:10.1021/jp907979v](https://doi.org/10.1021/jp907979v)
13. N. R. Wilson *et al.*, Graphene oxide: Structural analysis and application as a highly transparent support for electron microscopy. *ACS Nano* **3**, 2547 (2009). [doi:10.1021/nm900694t](https://doi.org/10.1021/nm900694t) [Medline](#)
14. D. Pacilé *et al.*, Electronic properties and atomic structure of graphene oxide membranes. *Carbon* **49**, 966 (2011). [doi:10.1016/j.carbon.2010.09.063](https://doi.org/10.1016/j.carbon.2010.09.063)
15. R. Zangi, A. E. Mark, Monolayer ice. *Phys. Rev. Lett.* **91**, 025502 (2003). [doi:10.1103/PhysRevLett.91.025502](https://doi.org/10.1103/PhysRevLett.91.025502) [Medline](#)
16. N. Giovambattista, P. J. Rossky, P. G. Debenedetti, Phase transitions induced by nanoconfinement in liquid water. *Phys. Rev. Lett.* **102**, 050603 (2009). [doi:10.1103/PhysRevLett.102.050603](https://doi.org/10.1103/PhysRevLett.102.050603) [Medline](#)
17. J. K. Holt *et al.*, Fast mass transport through sub-2-nanometer carbon nanotubes. *Science* **312**, 1034 (2006). [doi:10.1126/science.1126298](https://doi.org/10.1126/science.1126298) [Medline](#)

18. M. Majumder, N. Chopra, R. Andrews, B. J. Hinds, Nanoscale hydrodynamics: enhanced flow in carbon nanotubes. *Nature* **438**, 44 (2005). [doi:10.1038/438044a](https://doi.org/10.1038/438044a) [Medline](#)
19. X. Peng, J. Jin, Y. Nakamura, T. Ohno, I. Ichinose, Ultrafast permeation of water through protein-based membranes. *Nat. Nanotechnol.* **4**, 353 (2009). [doi:10.1038/nnano.2009.90](https://doi.org/10.1038/nnano.2009.90) [Medline](#)
20. X. Qin, Q. Yuan, Y. Zhao, S. Xie, Z. Liu, Measurement of the rate of water translocation through carbon nanotubes. *Nano Lett.* **11**, 2173 (2011). [doi:10.1021/nl200843g](https://doi.org/10.1021/nl200843g) [Medline](#)
21. M. Whitby, N. Quirke, Fluid flow in carbon nanotubes and nanopipes. *Nat. Nanotechnol.* **2**, 87 (2007). [doi:10.1038/nnano.2006.175](https://doi.org/10.1038/nnano.2006.175) [Medline](#)
22. J. C. Rasaiah, S. Garde, G. Hummer, Water in nonpolar confinement: From nanotubes to proteins and beyond. *Annu. Rev. Phys. Chem.* **59**, 713 (2008). [doi:10.1146/annurev.physchem.59.032607.093815](https://doi.org/10.1146/annurev.physchem.59.032607.093815) [Medline](#)
23. J. Köfinger, G. Hummer, C. Dellago, Macroscopically ordered water in nanopores. *Proc. Natl. Acad. Sci. U.S.A.* **105**, 13218 (2008). [doi:10.1073/pnas.0801448105](https://doi.org/10.1073/pnas.0801448105) [Medline](#)
24. J. A. Thomas, A. J. H. McGaughey, Water flow in carbon nanotubes: Transition to subcontinuum transport. *Phys. Rev. Lett.* **102**, 184502 (2009). [doi:10.1103/PhysRevLett.102.184502](https://doi.org/10.1103/PhysRevLett.102.184502) [Medline](#)
25. Y. Li, J. Xu, D. Li, Molecular dynamics simulations of nanoscale liquid flows. *Microfluid. Nanofluid.* **9**, 1011 (2010). [doi:10.1007/s10404-010-0612-5](https://doi.org/10.1007/s10404-010-0612-5)
26. F. Caupin, M. W. Cole, S. Balibar, J. Treiner, Absolute limit for the capillary rise of a fluid. *Europhys. Lett.* **82**, 56004 (2008). [doi:10.1209/0295-5075/82/56004](https://doi.org/10.1209/0295-5075/82/56004)
27. A. I. Livshits, M. E. Notkin, V. I. Pistunovich, M. Bacal, A. O. Busnyuk, Superpermeability: Critical points for applications in fusion. *J. Nucl. Mater.* **220-222**, 259 (1995). [doi:10.1016/0022-3115\(94\)00424-2](https://doi.org/10.1016/0022-3115(94)00424-2)
28. N. Goedecke, J. Eijkel, A. Manz, Evaporation driven pumping for chromatography application. *Lab Chip* **2**, 219 (2002). [doi:10.1039/b208031c](https://doi.org/10.1039/b208031c) [Medline](#)
29. W. S. Hummers Jr., R. E. Offeman, Preparation of graphitic oxide. *J. Am. Chem. Soc.* **80**, 1339 (1958). [doi:10.1021/ja01539a017](https://doi.org/10.1021/ja01539a017)
30. L. Greenspan, Humidity fixed points of binary saturated aqueous solutions. *J. Res. Natl. Bur. Stand. Sec. A* **81A**, 89 (1977).
31. R. T. Ferrell, D. M. Himmelblau, Diffusion coefficients of hydrogen and helium in water. *AIChE J.* **13**, 702 (1967). [doi:10.1002/aic.690130421](https://doi.org/10.1002/aic.690130421)
32. J. A. Thomas, A. J. McGaughey, Reassessing fast water transport through carbon nanotubes. *Nano Lett.* **8**, 2788 (2008). [doi:10.1021/nl8013617](https://doi.org/10.1021/nl8013617) [Medline](#)
33. U. Raviv, P. Laurat, J. Klein, Fluidity of water confined to subnanometre films. *Nature* **413**, 51 (2001). [doi:10.1038/35092523](https://doi.org/10.1038/35092523) [Medline](#)
34. S. H. Khan, G. Matei, S. Patil, P. M. Hoffmann, Dynamic solidification in nanoconfined water films. *Phys. Rev. Lett.* **105**, 106101 (2010). [doi:10.1103/PhysRevLett.105.106101](https://doi.org/10.1103/PhysRevLett.105.106101) [Medline](#)

35. K. Erickson *et al.*, Determination of the local chemical structure of graphene oxide and reduced graphene oxide. *Adv. Mater.* **22**, 4467 (2010). [doi:10.1002/adma.201000732](https://doi.org/10.1002/adma.201000732)  
[Medline](#)
36. <http://lammmps.sandia.gov>
37. H. J. C. Berendsen, J. R. Grigera, T. P. Straatsma, The missing term in effective pair potentials. *J. Phys. Chem.* **91**, 6269 (1987). [doi:10.1021/j100308a038](https://doi.org/10.1021/j100308a038)
38. P. Hirunsit, P. B. Balbuena, Effects of confinement on water structure and dynamics: A molecular simulation study. *J. Phys. Chem. C* **111**, 1709 (2007). [doi:10.1021/jp063718v](https://doi.org/10.1021/jp063718v)